The Flow Structure During Onset and Developed States of Rotating Stall Within a Vaned Diffuser of a Centrifugal Pump

Manish Sinha
Ali Pinarbasi
Joseph Katz

Department of Mechanical Engineering,
The Johns Hopkins University,
Baltimore, MD 21218

Particle Image Velocimetry (PIV) and pressure fluctuation measurements are used for investigating the onset and development of rotating stall within a centrifugal pump having a vaned diffuser. The experiments are performed in a facility that enables measurements between the diffuser vanes, within part of the impeller, in the gap between them and in the volute. The diffuser is also instrumented with pressure transducers that track the circumferential motion of rotating stall in the stator. The timing of low-pass-filtered pressure signals are also used for triggering the acquisition of PIV images. The data include detailed velocity distributions, instantaneous and phase-averaged, at different blade orientations and stall phases, as well as auto- and cross-spectra of pressure fluctuations measured simultaneously in neighboring vane passages. The cross-spectra show that the stall propagation rate is 0.93 Hz, 6.2 percent of the impeller speed, and that the stall travels from the passages located on the exit side of the volute toward the beginning side, crossing the tongue region in the same direction as the impeller, where it diminishes. Under stall conditions the flow in the diffuser passage alternates between outward jetting, when the low-pass-filtered pressure is high, to a reverse flow, when the filtered pressure is low. Being below design conditions, there is a consistent high-speed leakage flow in the gap between the impeller and the diffuser from the exit side to the beginning of the volute. Separation of this leakage flow from the diffuser vane causes the onset of the stall. The magnitude of the leakage and the velocity distribution in the gap depend on the orientation of the impeller blade. Conversely, the flow in a stalled diffuser passage and the occurrence of stall do not vary significantly with blade orientation. With decreasing flow-rate the magnitudes of leakage and reverse flow within a stalled diffuser passage increase, and the stall-cell size extends from one to two diffuser passages.
[DOI: 10.1115/1.1374213]

1 Introduction

At reduced flow rates, the performance, flow rate, and pressure of a compressor or a pump become increasingly unstable. When substantial flow fluctuations are propagating at a low frequency along the circumference, but are limited to parts of components (e.g., rotor, diffuser, or volute), the phenomenon is typically referred to as rotating stall. In spite of considerable efforts devoted to the study of rotating stall in compressors and pumps, the mechanics of this phenomenon are not yet well understood. Emmons et al. [1] provide a coherent explanation of rotating stall using cascade theory. While rotating stall may occur in any turbomachine, the phenomenon is most frequently observed and studied in compressors with a large number of blades. Its occurrence has also been reported in the impeller and in the diffuser/volute of centrifugal pumps (e.g., Lenneman and Howard [2]) with specific geometries. In a more recent research Yoshida et al. [3] investigate the rotating stall instability in a 7-bladed centrifugal impeller with a variety of diffusers. They observe that multiple stall cells occur, both in the impeller and in the vaned diffuser. The stall propagation speed in the diffuser is less than 10 percent of the impeller speed and is most evident when the clearance between impeller and diffuser vanes is large. In the present study, we examine the occurrence of stall in a centrifugal pump with a vaned diffuser that has a gap of 20 percent of the impeller radius and 15.4 percent of the diffuser chord length. This gap is larger than most of the available data for pumps.

Ogata et al. [4] report on measurements of pressure fluctuations and velocity fields, using hot wire measurements, in a vane diffuser of a centrifugal compressor. They conclude that the presence of a volute casing causes circumferentially nonuniform conditions at the outlet from the diffuser and that this nonuniformity is a large factor in the inception of rotating stall. Their velocity measurements indicate the existence of reverse flow in the vane passages with the lowest pressure field, but being point measurements, they cannot provide details on the flow structure and onset mechanisms. They also suggest that the propagation mechanism of a stall cell from one vane passage to another is more complex than the conventional explanation. Additional relevant reference material on stall and instabilities, including empirical correlations for the behavior of impellers and diffuser vanes can be found in Ribi [5], Tsujimoto [6], Miyake and Nagata [7] as well as Tsurusaki and Kinoshita [8]. Some recent computational work is described, for example, by Cao et al. [9] and Longatte and Kueny [10].

In spite of these efforts, there is still very little experimental data on the detailed flow structures within a stalled centrifugal turbomachine, the mechanism causing the onset of stall as well as on the effects of blade orientation and flow rate on the flow structure within a stalled pump. In this paper we use PIV to measure the velocity distributions within a vaned diffuser, part of the impeller, the gap between the diffuser and the impeller, and within the volute of a stalled pump. The experimental setup and test

Contributed by the Fluids Engineering Division for publication in the JOURNAL OF FLUIDS ENGINEERING. Manuscript received by the Fluids Engineering Division October 27, 2000; revised manuscript received March 15, 2001. Associate Editor: Y. Tsujimoto.

procedures are described in Section 2. The present measurements cover regions located on both sides of the tongue (cut water). Conditionally sampled data using the signal of a pressure transducer located within the diffuser is used for studying characteristic flow structures at different phases of the stall (Section 3). Pressure signals from several transducers located in adjacent blade passages are also used for measuring the propagation of the stall. The measured propagation frequency is only 6.2 percent of the impeller speed, but the propagation speed varies from one blade to the next, and stops at the beginning of the volute. The measurements are performed at different impeller orientations and different flow rates, starting from conditions for which the diffuser is not stalled down to conditions for which the stall cell covers more than one diffuser passage simultaneously. We show that high-speed leakage (circumferential flow) in the gap between the diffuser and the impeller, from the exit side to the volute to the beginning side, plays a major role in causing the onset of stall. It is also shown that the flow in the vane passage alternates between outward jetting when the passage is not stalled to strong reverse flow in a stalled passage (or two passages, depending on flow rate).

2 Experimental Setup and Procedures

2.1 Setup. A schematic description of the centrifugal pump used in the present study is presented in Fig. 1 and relevant details on the pump geometry are presented in Table 1. The pump is vibration isolated and separated from the rest of the facility using 50 m of coiled flexible hoses. A converging nozzle and flow straighteners (honeycombs and screens) at the entrance to the pump insure smooth inflow into the impeller. Further details on the test loop can be found in Sinha and Katz [11] and Sinha et al. [12].

The impeller has backswept blades with a logarithmic profile and the vaned diffuser has straight walls with a constant cross section. The configuration (radius) of the perimeter of the volute, r_v, in cm is given by:

$$r_v = 17.78 + 24.46 \times (\theta/360) \quad (\theta \text{ varies between } 0°\text{-}360°).$$

In the present configuration the tip of the tongue is located at $\theta = 29$ deg. Beyond $\theta = 360$ deg the outer perimeter is straight. The 24.46×1.27 cm^2 exit is gradually expanded to a 10.16 cm pipe by imposing a maximum expansion angle of less than 7 deg to avoid separation. Parts of the original stainless-steel blades and outer shroud of the impeller were removed and replaced with acrylic to allow visual access in the flow within the impeller. The entire diffuser and outer perimeter of the volute are also transparent. This setup allows illumination, flow visualization, and PIV measurements in both the horizontal (parallel to the shrouds) and vertical (parallel to the shaft) planes. The pump is also instrumented with flush mounted piezoelectric pressure transducers (PCB 105B02) that are mounted on the hub surface, along the centerline, in six adjacent vane passages. They are labeled A–F in Fig. 1.

Table 1 Geometric data and operating conditions

Impeller:	
Inlet diameter	8.51 cm
Discharge diameter	20.32 cm
Number of blades	5 backswept
Exit angle of blade	21.3°
Diffuser:	
Number of vanes	9
Inside diameter	24.45 cm
Discharge diameter	30.5 cm
Inlet angle of vane	10.6°
Outlet angle of vane	10.97°
Chord length	13.44 cm
Suction side radius	14.15 cm
Pressure side radius	24.79 cm
Axial width	1.27 cm
Operating conditions:	
Rotor speed	890 rpm
Design flow rate	5.67 l/s
Design Flow coefficient, $\varphi = Q/\pi DBU_t$ Q is the flow rate, D, B and U_t are the impeller diameter, width and tip speed, respectively.	0.118
Design specific speed	0.49
Flow-rate during the present experiments	2.52 l/s – 3.78 l/s
Flow coefficient during the present experiments	0.052-0.078

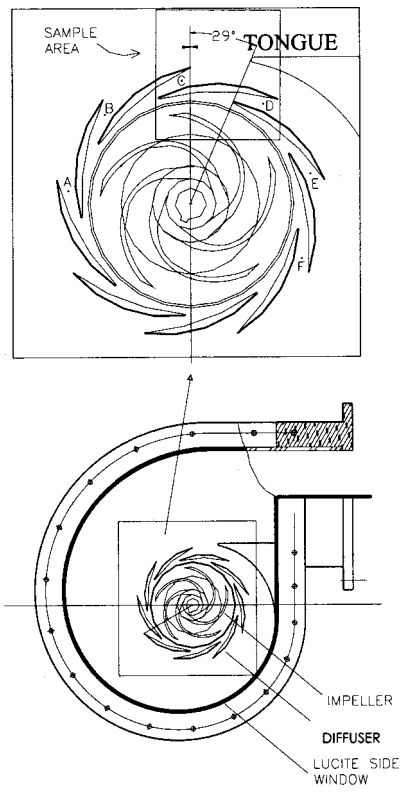

Fig. 1 The pump geometry and location of the present measurements

2.2 PIV system. All the data included in the present paper focus on the flow near the exit of the pump and the sample area is specified in Fig. 1. All the measurements are performed in the mid-section, i.e., in the 50 percent plane between the hub and the shroud. The optical setup of the PIV system is illustrated in Fig. 2. A 350 mJ/pulse, Nd-Yag laser and sheet forming optics are similar to the setup used in previous experiments [11,12] where one can find reference data on the flow at design conditions. The images are recorded by a 2048×2048 pixels, 4 frames/s digital camera that incorporates fast digital image shifting [11,12] to overcome directional ambiguity. The images are recorded at the desired impeller orientation using a shaft encoder. In addition, the electronic control unit provides trigger signals during maximum, minimum and zero-crossing phases of the low-pass-filtered signal of the transducer located at C (see Fig. 1). As will be shown in the next section, this signal is associated with the stall.

The acquired images are enhanced using an in-house histogram equalization algorithm and analyzed with in-house auto-correlation software [13–15]. The window size is 64×64 pixels

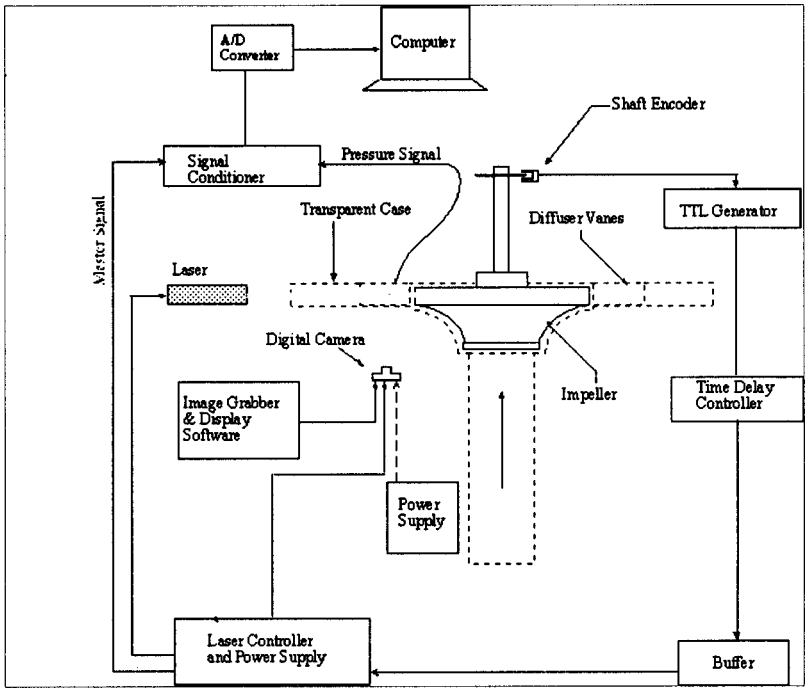

Fig. 2 The optical and control systems

and the vectors are calculated every 32 pixels, i.e., 50 percent overlap between neighboring windows. The water is seeded with 20 μm, neutrally buoyant fluorescent particles. The fluorescent particles enable us to install a high-pass filter in front of the camera that cuts the green laser light but allows unobstructed transmission of the yellow fluorescence. Consequently, reflections from solid boundaries, such as blades, vanes, and shrouds do not obscure the particles' traces, even very close to the blade surfaces. The uncertainty has been determined, calibrated, and discussed in detail in several of our previous papers (e.g., Dong et al. [16], Roth et al. [17], [13–15], Sridhar [18]). The standard deviation of the difference between the exact and measured velocities in both experimental and computer-generated images has been found to be about 0.2 pixels, provided there are sufficient number of particles per interrogation window. Consequently, the uncertainty in velocity measurements is in the 0.2–0.4 pixels range (depending on how stringent one chooses to be) and we have opted to use 0.3 pixels as a characteristic value. To achieve this uncertainty the particle concentration must be maintained at a level that ensures a distribution of at least 7—8 image pairs per interrogation window. This requirement is consistent with results of other studies of uncertainty in PIV measurements (Adrian [19]). Consequently, for a characteristic displacement of 20 pixels between exposures, the uncertainty is about 1.5 percent.

3 Results

3.1 Performance, Pressure Fluctuations and Propagation Rate. A performance curve of the present pump is presented in Fig. 3. At flow coefficients below 0.06 there is a change in the slope of the performance curve and as a result it is believed that the pump is close to the onset condition of rotating stall. Sample power spectra of the pressure signals in passage C under conditions of stall and no-stall are presented in Fig. 4(*a*). The pump shaft frequency is 14.83 Hz, but at this frequency there is only a change in slope. The peaks at twice and three times this frequency on design conditions are clear. There are five impeller blades, which means that the frequency at which blades pass by the same vane passage is 74.2 Hz. The largest peak in Fig. 4(*a*) (on design conditions) corresponds to this passing frequency. Its first super harmonic at 148.4 Hz is also evident. There are nine diffuser vanes, which means that the rate at which the same impeller blade passes by the diffuser vanes is 133.5 Hz. There is a clear spectral peak at this frequency too. There is another peak at ~122 Hz that we cannot explain and the reasons for its occurrence are beyond the scope of this paper. Under stalled conditions the peaks at 29.6, 74.2, 122, and 133.5 Hz are smaller, but they are higher at 44.5 Hz and at frequencies below 14.8 Hz. In particular, there is an increase of about 5 db below 1 Hz. Under a stalled condition, the power spectrum in fact yields an additional peak at 0.93 Hz in the signals of the transducers in passages A, B, C, D, and E, but not in the signal of transducer F. Samples of auto-spectra for passages, A, B, E, and F are presented in Fig. 4(*b*). The spectra for passages C and D are not shown since they are almost identical to those in passages A and B. Clearly, unlike passages A–E, there is no distinct spectral peak at frequencies below 15 Hz in passage F.

Figure 5(*a*) shows a sample of the magnitude of the cross-spectrum between the pressure signals A and B, and Fig. 5(*b*) provides the phase information A similar analysis was performed

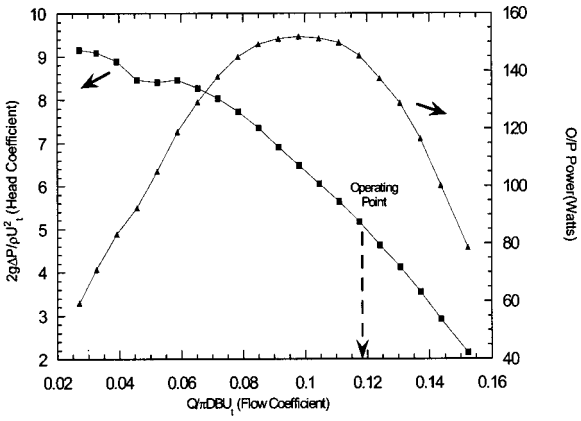

Fig. 3 The performance curve (squares) and output power (triangles) of the pump

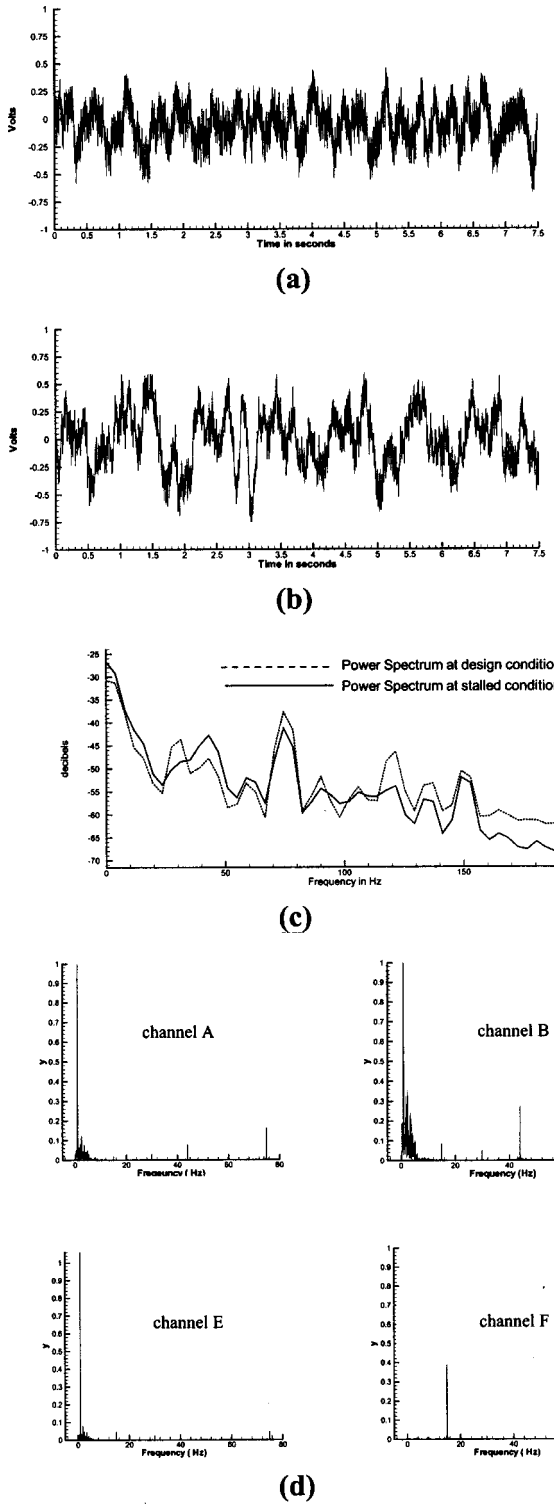

Fig. 4 A typical pressure signal of transducer C at: (*a*) design conditions (φ=0.118), (*b*) stalled conditions (φ=0.062), (*c*) power spectra of the signals in 4(*a*) and 4(*b*), (*d*) auto spectrum of Channels A, B, E, and F

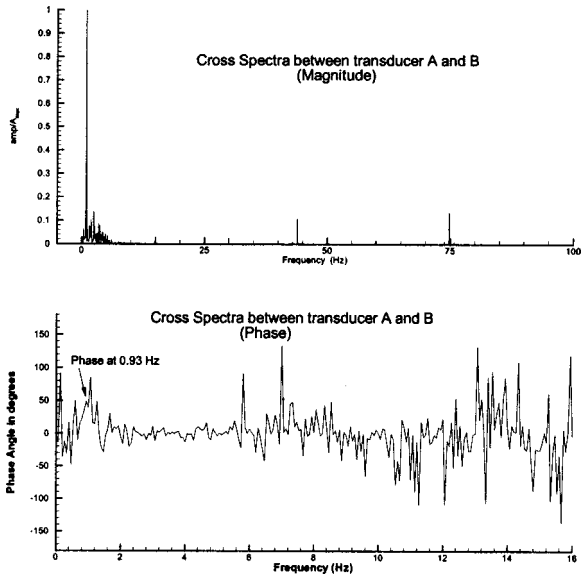

Fig. 5 (*a*) Sample cross spectrum magnitude of transducer signals in vane passages A and B; (*b*) phase difference between the signals of tranducers A and B

between each pair of transducer signals. The peaks are at frequencies that are common to the two signals and the phase is indicative of the time lag/lead between them. We obtain data at 0.93 Hz for passages ''A''-''E,'' since there is no peak in the spectra involving passage ''F.'' The phase angles by which the pressure signal of sensor ''A'' leads the signals in the other passages are tabulated in Table 2.

Clearly, the time delay varies as the phenomenon moves from one passage to another. The propagation speed initially increases as the tongue is approached. The time lag between sensor A and B is 0.145 s, whereas the lag between B and C is 0.06 s. Between C and D the lag increases only slightly to 0.08 s, but then it increases substantially to 0.44 s between D and E and disappears completely in F. The decaying propagation speed suggests the influence of the non-uniform flow conditions (circumferential pressure gradients) that exist, according to Ogata et al. [4], in the volute casing outside the diffuser, or in the gap between the impeller and the diffuser, as the present velocity measurements indicate. Since the propagation speed is not uniform we cannot use the Hanover diagram (Japikse et al. [20]) for estimating the number of stalled cells that exist at a given instant of time.

RMS values of pressure fluctuation in passages A–F, are recorded at different flow rates, starting from 5.67 1/s and lower (Fig. 6). The rms values start increasing at around 3.78 1/s in channels A, B, C, D, and E. The pressure fluctuations at D are initially lower than the levels in the other passages and it starts to rise at the same flow rate. However, it continues to rise well after the signals at A, B, C, and E reach maximum levels and peaks only at about 2.84 1/s. For the A–E passages, the rms levels decrease to a lower, but still elevated, levels below 2.75 1/s. Passage F does not follow the same trend. There, the fluctuations remain at almost the same level until 2.75 1/s where there is a sharp increase followed by an immediate decrease to an elevated

Table 2 Measured phase and time lead at 0.93 Hz obtained from cross-spectra of the pressure signals in passages A, B, C, D, and E. Transducer F has no peak at 0.93 Hz.

Transducers:	A&B	A&C	A&D	A&E	A&F
Angular separation	40.0 deg	80.0 deg	120.0 deg	160.0 deg	200.0 deg
Phase lead	48.49 deg	68.59 deg	94.06 deg	258.0 deg	not stalled
Time lead (s)	0.145	0.205	0.281	0.717	not stalled

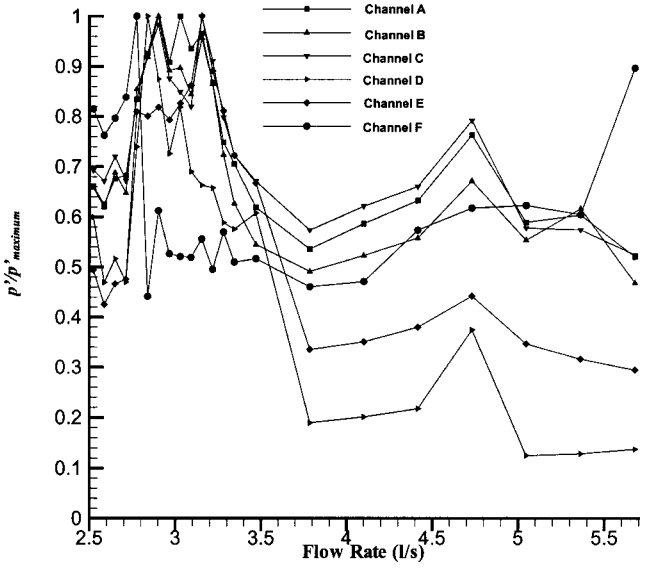

Fig. 6 RMS values of pressure fluctuations as a function of flow rate

level. Thus, at 3 1/s (φ=0.062) passages A, B, C, D, E are experiencing high pressure fluctuations whereas passage F is not. Consistent with the spectral analysis, and confirmed by the velocity distributions, discussed in the next section, the increased level of fluctuation is caused by massive flow oscillations, from being stalled (reverse flow) to having a jet flowing through (forward outflow) in the vane passage. Since the increase in pressure fluctuations begins at around 3.78 1/s, to study the onset of stall PIV images are recorded at and below 3.78 1/s, down to 2.52 1/s. We record data when the stall related, low-pass-filtered, pressure signal is maximum, minimum and during zero crossing (growth or decay). Reference data on the flow in other vane passages when the pump operates on design conditions can be found in Sinha et al. [11,12].

3.2 Flow Structures at Different Phases. Sample instantaneous vector maps at different phases of the stall, when the low-pass-filtered transducer signal at C is minimum, during zero crossing and maximum, all at φ=0.062, are presented in Figs. 7(*a*–*c*), respectively. The blade orientation is the same in all three cases. At minimum pressure, there is a reverse flow in van passage C. The magnitude of reverse velocity is only about 10 percent of the impeller tip speed. There is also clear evidence of flow separation at the trailing edge of the vane. During zero crossing (Fig. 7(*b*), i.e., as the pressure in C is rising, the flow in passage C is in the process of recovering from the reverse flow, whereas there is still backward flow in passage D above it. Interestingly, in Fig. 7(*b*) there is a negative radial velocity on the pressure side of the impeller blade, i.e., there is a backward flow into the impeller.

At a pressure-maximum phase, there is a strong outward flow (Fig. 7(*c*)) through passages C and D. The velocity at D is higher, presumably due to the lower mean pressure at the beginning of the volute when the pump operates below design conditions. The outflow from passage C separates from the convex side of the vane and is aimed directly toward the exit. In all cases there is a strong leakage flow in the gap between the impeller and the diffuser from the exit side to the beginning of the volute. The leakage velocity exceeds 50 percent of the impeller tip speed. The secondary flow downstream of the diffuser is complex but is significantly slower.

3.3 Effect of Blade Orientation. Figure 8(*a*–*c*) and Fig. 9(*a*–*c*) show sample phase averaged data (averages of 10 images, each) during minimum and maximum pressure phases, at 3 different impeller orientations, −4 (356), 26, and 56 deg, respectively. A complete set, every 10 deg, can be found in Sinha [21].

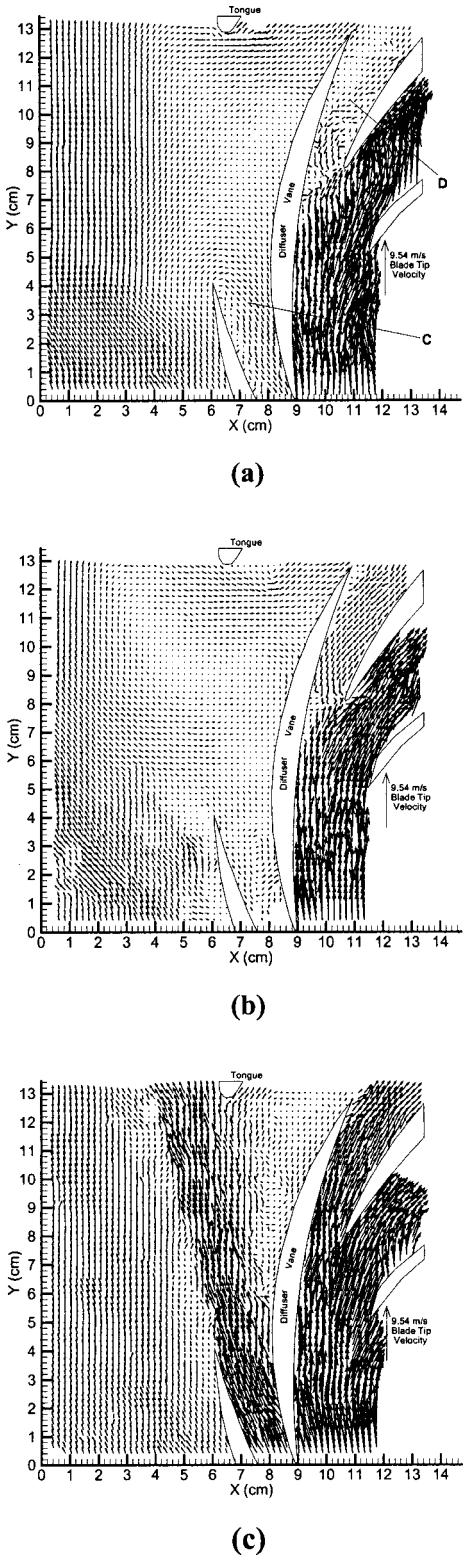

Fig. 7 Sample Instantaneous velocity maps at: (*a*) minimum, (*b*) zero-crossing (on the rise), and (*c*) maximum phases of the low-pass-filtered pressure signal at passage C (φ=0.062)

At minimum pressure-phase (Fig. 8), the phase-averaged data shows a reverse flow into passage C and a slow outward flow in passage D. As the flow turns around back into the passage C it

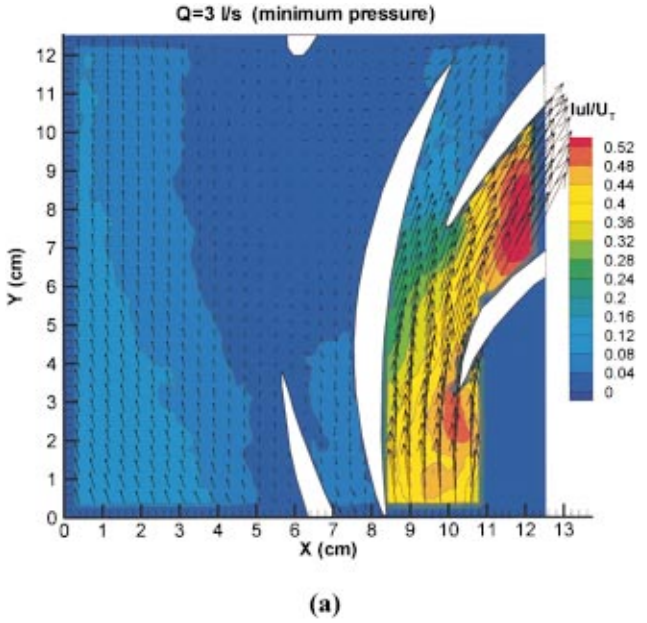

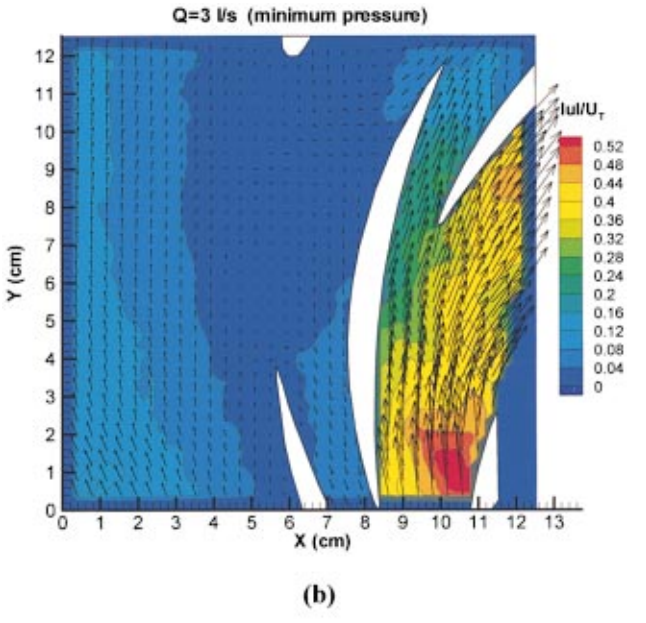

Fig. 8 Phase averaged velocity maps at a minimum pressure phase when the blade is at: (*a*) −4 deg, (*b*) 26 deg, and (*c*) 56 deg. The colors indicate velocity magnitude and a reference vector is provided in Fig. 7. Only alternate vectors are shown for clarity.

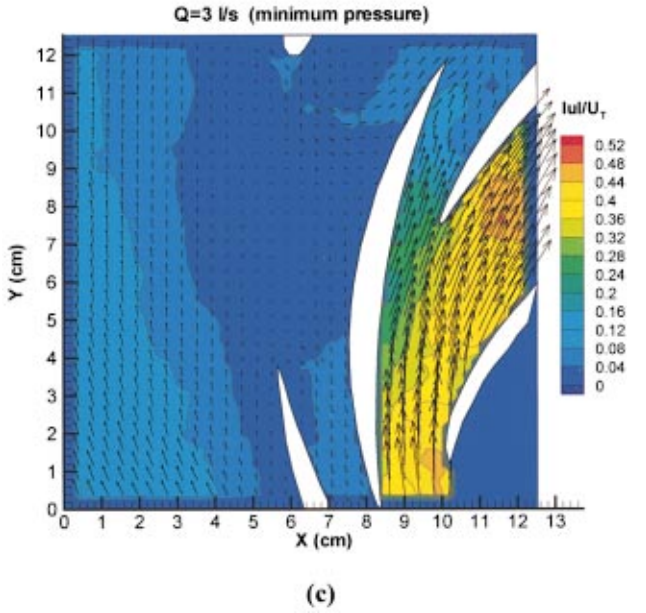

Fig. 8 (*Continued*)

separates near the trailing edge of the lower diffuser vane, creating a pocket of no flow at the trailing edge, on the concave side of the lower vane. Several relatively weak vortex structures/large eddies can also be seen outside of the diffuser, in the vicinity of the tongue. Between instantaneous realizations these eddies vary both in strength and spatial locations.

As indicated before, the most dominant phenomenon is the high speed-leakage flow between the impeller and the diffuser, from the exit side of the pump (left side of the tongue) toward the beginning of the volute. The magnitude of the phase-averaged leakage velocity also exceeds 50 percent of the impeller tip speed. The magnitude and orientation of the leakage flow varies with blade orientation due to the ''jetting'' in the pressure side of the impeller blade and the ''wake'' region behind the blade. The impeller orientation, still at minimum pressure phase, also affects the out flux from passage D. It is at maximum in Fig. 8(*b*), when the vane passage faces the pressure side of the blade, and minimum in Fig. 8(*a*), when passage D is exposed to the suction side of the blade. Conversely, the phase-averaged flow outside of the diffuser is very slow, with very little secondary flow from the exit side to the beginning of the volute or from the beginning to the exit side. This trend indicates that the circumferential pressure gradients causing the leakage flow are confined to the narrow gap between the impeller and the diffuser. The pressure gradients outside of the diffuser are weak.

At a maximum pressure phase (Fig. 9), there is an outward jet from the vane passage with velocity magnitude of about 60 percent of the typical values on design condition (available in Sinha and Katz [11]). The jet is aimed directly toward the exit and there is no indication that it is affected by circumferential pressure gradients in the volute. The jet velocity is slightly higher when vane passage C is exposed to the pressure side of the blade (Fig. 9(*a*)), and the separation point on the convex side of the diffuser vane (separating passages C and D) shifts as the impeller blade passes by, but these fluctuations are small. There is essentially no (phase-averaged) flow to the right of the jet and the tongue. The out flux from passage D also increases when the inlet to this passage is exposed to the pressure side of impeller blade (Fig. 9(*b*)).

In the gap between the impeller and diffuser the fast leakage flow persists in the maximum pressure phase of the stall. In fact, the characteristic leakage velocity is even higher than that of the minimum pressure phase. The velocity distribution depends, but not to a great extent, on the orientation of the impeller. The velocity is typically higher, exceeding 50 percent of the tip speed, on the pressure side of the impeller blade (ahead of the tip), and decreases as much as 40–45 percent in other regions. The decrease is particularly evident when the blade is located near the diffuser vane separating passages D and E (Fig. 9(*a*)). In summary, it is shown that the phase-averaged flow structure under stalled conditions shows some, but not substantial, dependence on the impeller orientation. Most of the effects are confined to the immediate vicinity of the blade (which is not surprising) and there is limited impact on the flow within the diffuser during maximum pressure phase. A probable cause for this limited effect is the high speed circumferential leakage flow that separates between the impeller and the diffuser.

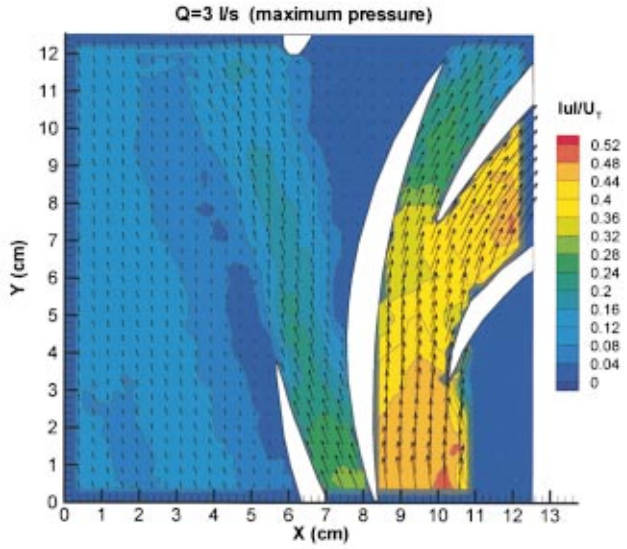

(a)

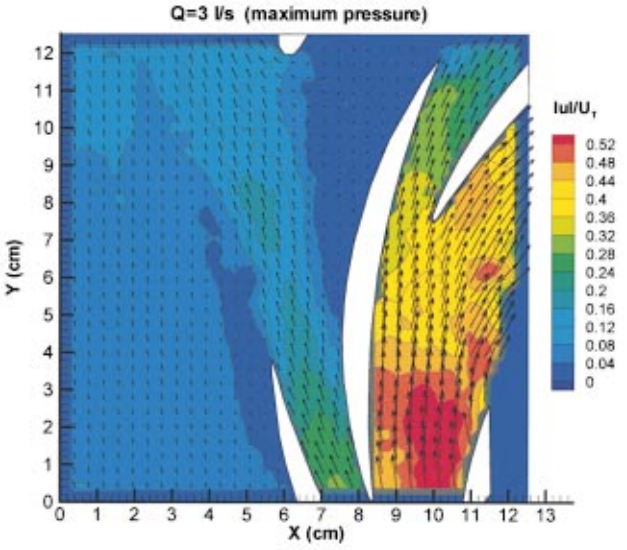

(b)

Fig. 9 Phase averaged velocitiy maps at a minimum pressure phase when the blade is at: (*a*) −4 deg, (*b*) 26 deg, and (*c*) 56 deg. The colors indicate velocity magnitude and a reference vector is provided in Fig. 7. Only alternate vectors are shown for clarity.

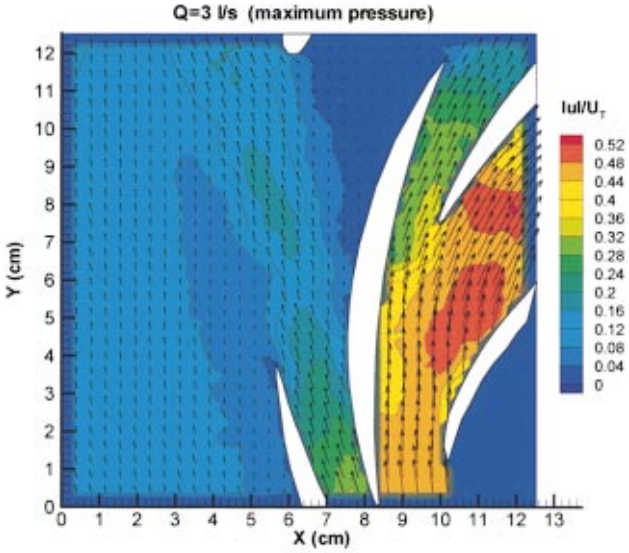

(c)

Fig. 9 (*Continued*)

3.4 Effect of Flow Rate and Onset of Stall. Figures 10(*a*,*b*)–13(*a*,*b*) contain representative samples of instantaneous and phase averaged velocity maps (this time an average of 20 each) at 3.78 1/s (φ=0.078), 3.28 1/s (φ=0.068), 3.02 1/s (φ=0.062), and 2.52 1/s (φ=0.052), respectively, all at a minimum pressure phase and at the same blade orientation. These four characteristic examples are selected from an available series of 11 sets that covers the range φ=0.052–0.078 available in Sinha [21]. They are selected to demonstrate the transition, with decreasing flow rate, from a flow that is not stalled to conditions of massive stall that covers more than one blade passage simultaneously. In all cases the flow is below design conditions. As Figs. 3 and 6 indicate, at φ=0.078 (the upper bound), the flow is clearly not stalled. This condition is still far from the local minimum in performance curve and the pressure fluctuations are still relatively low. With decreasing flow rate there is a range of conditions with high pressure fluctuations that are caused by the rotating stall. The highest fluctuations occur at $\varphi\sim$0.062. As the flow is decreased further the pressure fluctuations decrease again. The lower bound of our range of samples, φ=0.052, is already well below the range of flow rates with high pressure fluctuations. The latter is also close to the local minimum in the performance curve.

Typical narrow jetting near the concave side of the vane with a wide separated region in the convex side dominate the flow in and downstream of the diffuser at 3.78 1/s (φ=0.078), as shown in Fig. 10(a,b). At this flow rate the outward jet always exists. Part of the jet exiting from the previous diffuser passage (passage B), 40 deg upstream, is also evident, both in the instantaneous and phase averaged velocity distributions. This phenomenon is similar to that shown by Johnston and Dean [22] for off-design flow rates and similar (but lower velocity) to the phenomena occurring at higher flow rates in this pump [11] . Note also that there is a secondary flow from the beginning side of the volute (right of the tongue) toward the exit. This phenomenon indicates that the pressure gradients near the tongue are in the opposite direction compared to the gradients in the gap between the impeller and the diffuser, where the flow leaks to the beginning of the volute. The secondary flow around the tongue disappears at lower flow rates.

With decreasing flow rate the characteristic jet velocity decreases and the traces of the jet from passage B eventually disappear. Conversely, the leakage flow increases substantially, as is evident by comparing the samples in Fig. 10–13. In addition, the velocity in the outer sections of the volute (low x in the examples shown) becomes consistently higher than the flow in the vicinity of the tongue, a trend that is characteristic to operation off design conditions [16]. At about φ=0.068 the flow in passage C stops intermittently and even becomes negative, but the phase-averaged flow is still positive (Fig. 11(*b*)). In Fig. 11(*a*) the flow through passage D is positive, and quite fast, and there are traces of the jetting from passage B. Thus, only passage C is stalled, which is characteristic to the size of the stall cell at this flow rate.

The frequency of reverse flow increases with decreasing flow rate and eventually even the phase-averaged velocity in passage C becomes negative (Fig. 12(*b*)) during minimum pressure phase. At and below φ=0.065 (data not shown–the pattern is similar to Fig. 12(*a*,*b*)) the instantaneous stalled area starts covering two diffuser vane passages intermittently although the phase average distribution only covers one passage. The reverse flow magnitude also

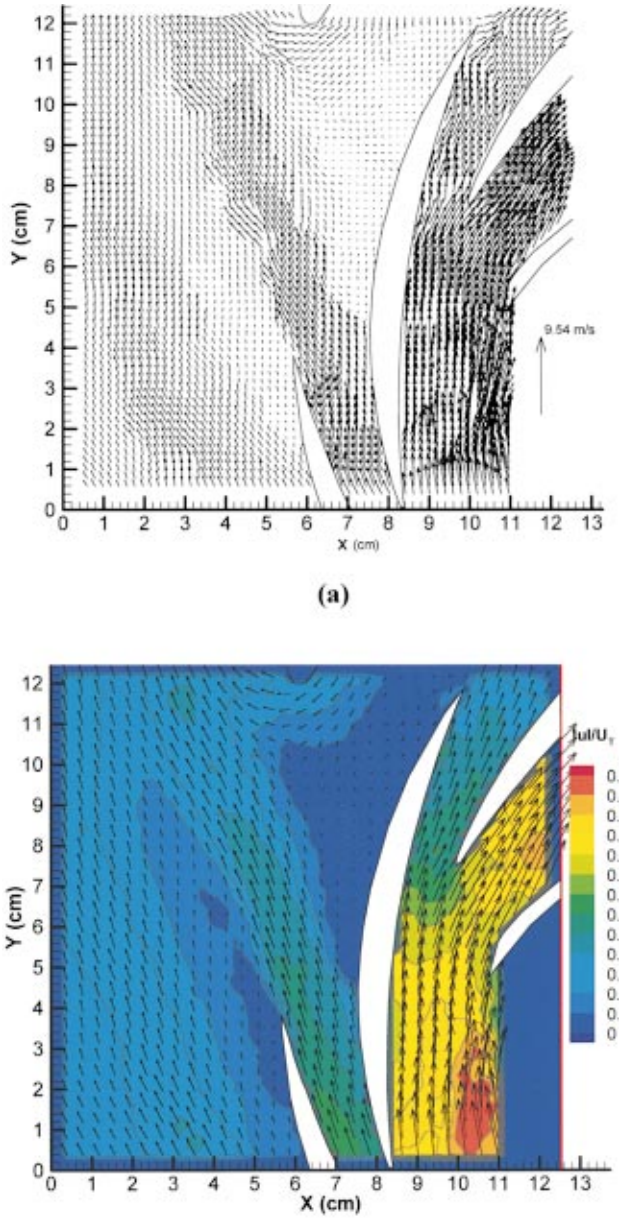

Fig. 10 Sample (*a*) instantaneous; and (*b*) phase averaged velocity maps (only alternate vectors are shown in *b*) at a minimum pressure phase. The flow rate is 3.78 1/s (φ=0.078) and the blade orientation is 6 deg.

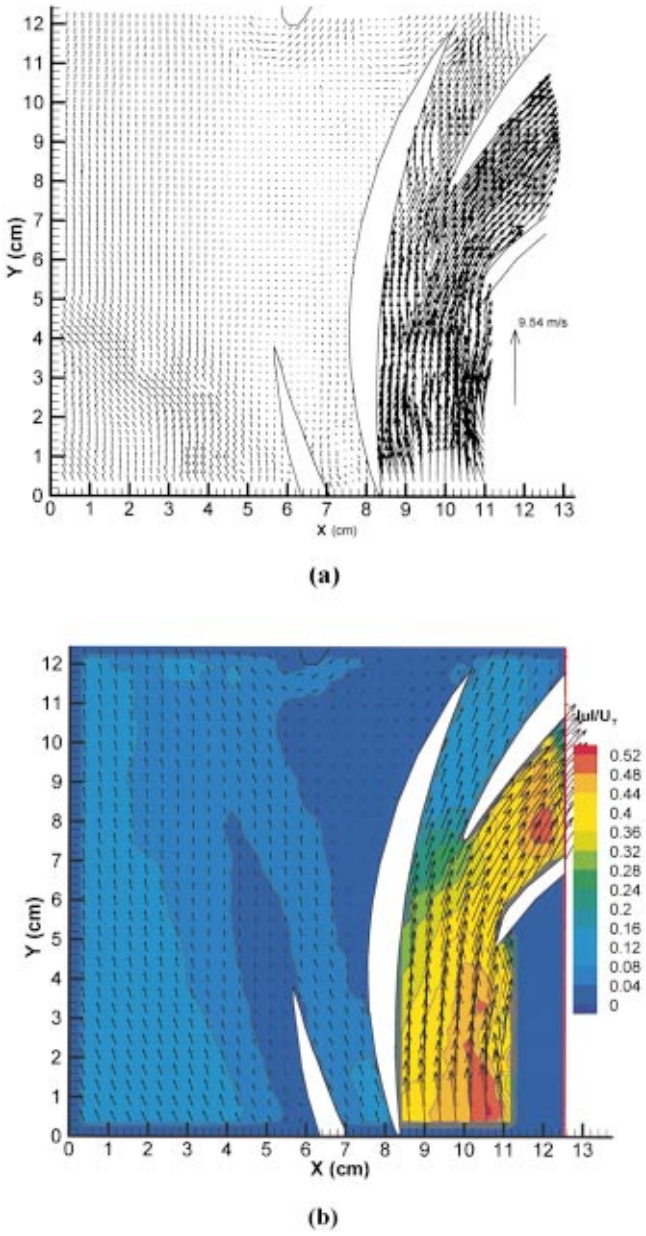

Fig. 11 Sample (*a*) instantaneous and (*b*) phase averaged velocity maps (only alternate vectors are shown in *b*) at a minimum pressure phase. The flow rate is 3.28 1/s (φ=0.068) and the blade orientation is 6 deg.

continues to increase. At φ=0.062 reverse flow regularly occurs in passage C during minimum pressure phase and at φ=0.052 (Fig. 13) the flow is consistently reversed in both passages C and D. Consequently, even the phase-averaged flow is negative.

Before concluding, it is of interest to identify exactly where the stall process starts. Our ability is limited since all the velocity measurements are performed in the same central plane and the flow is three-dimensional. A clear illustration that the flow is three-dimensional is the fact that the backward flow into passage D in Fig. 12(*a*) faces a flow in the opposite direction at the entrance to the passage. Obviously, to satisfy continuity there has to be a flow in the opposite direction in other planes. However, examination of the velocity distributions as the stall develops provides sufficient information to follow the process. As an illustration, let us examine the flow in passage D in Fig. 14 (φ=0.059) that shows a characteristic velocity distribution during early stages of transition from forward to reverse flow in the passage. In this example, the flow is separated on the concave surface but there is still an outward flow along the convex surface. The same trend, i.e., that the stall starts as the flow separates on the concave side of the passage, occurs also in passage C but typically at higher flow rate, due to the location of the trigger transducer. This phenomenon is most likely associated with the fast leakage flow that makes a turn near the narrowest point of the diffuser. Combined with the adverse pressure gradients in the passage (especially during a minimum pressure phase) the concave surface becomes prone to massive flow separation and stalling. As a vane passage stalls the leakage velocity increases which further increases the pressure gradients at the point where the leakage flow turns at the entrance to a passage. Thus, stalling of passage C increases the likelihood of subsequent stalling of passage D, i.e., a rotating stall. This process stops when the pressure gradients in a passage become favorable for outward flow. Due to the circumferential pres-

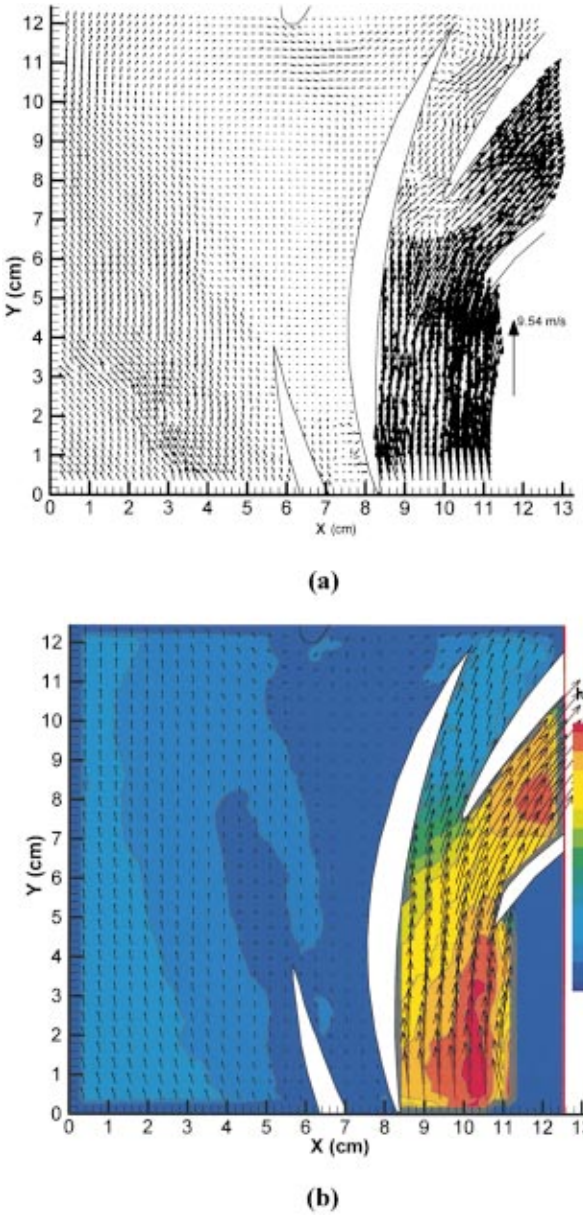

Fig. 12 Sample (*a*) instantaneous and (*b*) phase averaged velocity maps (only alternate vectors shown in *b*) at a minimum pressure phase. The flow rate is 3.08 1/s (φ=0.062) and the blade orientation is 6 deg.

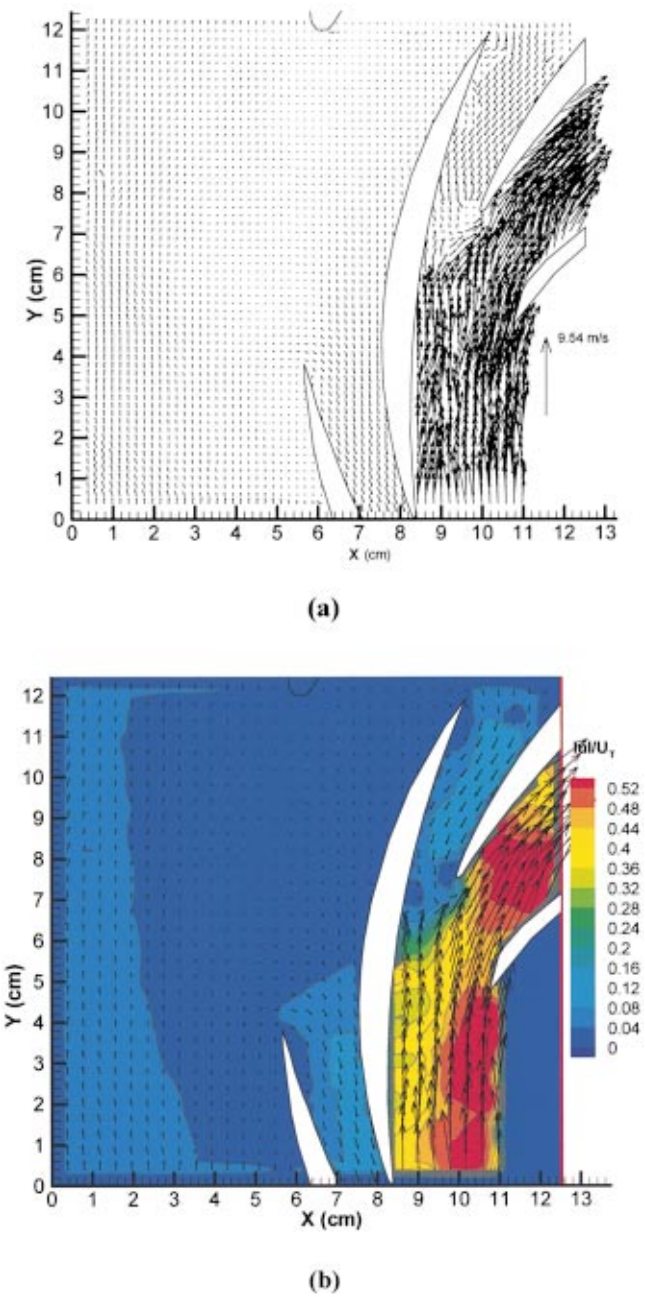

Fig. 13 Sample (*a*) instantaneous and (*b*) phase averaged velocity maps (only alternate vectors are shown in *b*) at a minimum pressure phase. The flow rate is 2.52 1/s (φ=0.052) and the blade orientation is 6 deg.

sure gradients below design conditions (Iversen et al. [23], [14,16], that in the present pump seem to be confined to the gap between the impeller and the diffuser, eventually the leakage flow finds a passage (most likely passage F above 2.8 1/s) where it can flow out. Consequently, in the present pump, passage F is not stalled at 3.02 1/s, as the spectral analysis demonstrates.

4 Summary and Conclusions

PIV and pressure fluctuation measurements are used for studying the flow structure within a centrifugal pump with a vaned diffuser under stall conditions. Cross spectra of the pressure signals at neighboring passages, as well as the RMS levels of pressure fluctuations confirms that a rotating stall occurs at a frequency of 0.93 Hz, 6.2 percent of the impeller speed. The stall is detected at the exit side of the pump and propagates with varying speeds to the beginning side, where it is quenched. The quenching of the stall occurs in a vane passage at the beginning of the volute where the pressure gradients for outflow are more favorable. Thus, unlike axial turbomachines, the circumferential pressure variations in the diffuser/volute confine the stall to a small part of the diffuser. This observation is consistent with the conclusions of Ogata et al. [4], that circumferential pressure nonuniformities affect the conditions for the onset of stall.

When the pump is stalled the flow in the diffuser passage alternates between an outward jetting, when the low-pass-filtered pressure signal in the vane passage is high, to a reverse flow, when the filtered pressure is low. Being below design conditions, there is a consistent high-speed leakage flow in the gap between the impeller and the diffuser from the exit side to the beginning of the volute. Separation of this leakage flow from the concave side of the diffuser vane causes the onset of the stall. The magnitude of

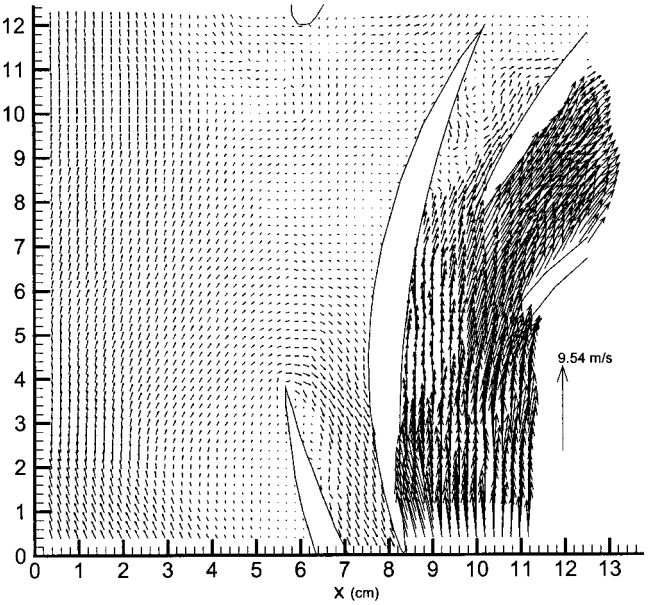

Fig. 14 Sample instantaneous velocity distribution at a minimum pressure phase as massive flow separation and the onset of stall occur in passage D. The flow rate is 2.89 1/s (φ=0.060) and the blade orientation is 6 deg.

the leakage and the velocity distribution in the gap depend on the orientation of the impeller blade. Conversely, the flow in a stalled diffuser passage does not vary significantly with impeller blade orientation. With decreasing flow-rate the magnitudes of leakage and reverse flow within a stalled diffuser passage increase and the stall-cell size extends from one to two diffuser passages. Unlike the gap between the impeller and the diffuser, there is very little leakage flow in the volute downstream of the diffuser, indicating that the circumferential pressure gradients in the volute are substantially smaller than those in the gap. This phenomenon is probably related to the uncharacteristic large gap between the impeller and the diffuser of the present pump (2.07 cm, 10.2 percent of the impeller diameter and 15.4 percent of the diffuser vane chord length). As indicated in Yoshida et al. [3], increasing the gap between the impeller and the diffuser also increases the likelihood and effect of the stall. Narrower gaps will not allow such a strong leakage flow in the gap, and will most likely thus ''push'' the circumferential pressure gradients and leakage into the volute.

Acknowledgment

This work has been funded in part by the Office of Naval Research through NSWC contract No: N000167-96-C-0086 (T. Calvert is program director at NSWC) and ONR grant No. N00014-98-1-0221 (P. Purtell, program officer) and in part by the Air Force Office of Scientific Research under grant No. F49620-97-1-0110 (T. Beutner, program director). We would also like to thank T. Calvert for providing the pump and S. King for construction of the electronics.

References

[1] Emmons, H. W., Kronauer, R. E., and Rockett, J. A., 1959, ''A survey of stall propagation–experiment and theory,'' ASME J. Basic Eng. **81**, pp. 409–416.
[2] Lennemann, E., and Howard, J. H. G., 1970, ''Unsteady flow phenomena in rotating centrifugal impeller passages,'' ASME J. Eng. Power **92**, 65–72.
[3] Yoshida, Y., Murakami, Y., Tsurusaki, T., and Tsujimoto, Y., 1991, ''Rotating Stalls in Centrifugal Impeller/Vaned Diffuser Systems,'' *Proc. First ASME/JSME Joint Fluids Engineering Conference*, **FED-107**, pp. 125–130.
[4] Ogata, M., and Ichiro A., 1995, ''An Experimental Study of Rotating Stall in a Radial Vaned Diffuser,'' *Unsteady Aerodynamics and Aeroelasticity of Turbomachines*, pp. 625–641.
[5] Ribi, B., 1996, ''Instability Phenomena in Centrifugal Compressors,'' *Flow in Radial Turbomachines*, Von Karman Institute Lectures series No. 1966-01, R. A. Van den Braembussche, ed.
[6] Tsujimoto, Y., 1996, ''Vaneless Diffuser Rotating Stall and Its Control,'' *Flow in Radial Turbomachines*, Von Karman Institute Lecture series No. 1996-01, R. A. Van den Braembussche, ed.
[7] Miyake, Y., and Nagata, T., 1999, ''Full Simulation of a Flow in a Single Stage Axial-Rotor in Rotating Stall,'' FEDSM-7197, ASME Fluids Eng. Conf., San Francisco.
[8] Tsurusaki, H., and Kinoshita T., 1999, ''Flow Control of Rotating Stall in a Radial Vaneless Diffuser,'' FEDSM99-7199, ASME Fluids Eng. Conf., San Francisco.
[9] Cao, S., Goulas, A., Wu, Y., Tsukamoto, H., Peng, G., Liu, W., Zhao, L., and Cao, B., 1999, ''Three-Dimensional Turbulent Flow in a Centrifugal Pump Impeller Under Design and Off-Design Operating Conditions,'' FEDSM-6872 Proceedings of the ASME Fluids Engineering Division, July 18–23, San Francisco.
[10] Longatte F., and Kueny J. L., 1999, ''Analysis of Rotor Stator Circuit Interactions in a Centrifugal Pump,'' FEDSM-6866, ASME Fluids Eng. Conf., San Francisco.
[11] Sinha, M. and Katz, J., 2000, ''Quantitative Visualization of the Flow in a Centrifugal Pump with Diffuser Vanes, Part A: On Flow Structure and Turbulence,'' ASME J. Fluids Eng. **122**, No. 1, pp. 97–107.
[12] Sinha, M., Katz, J., and Meneveau, C., 2000, ''Quantitative Visualization of the Flow in a Centrifugal Pump with Diffuser Vanes, Part B: Addressing Passage-Averaged and LES Modeling Issues in Turbomachinery Flows,'' ASME J. Fluids Eng. **122**, No. 1, pp. 108–116.
[13] Roth, G., Mascenik, D. T., and Katz, J., 1999, ''Measurements of the Flow Structure And Turbulence Within A Ship Bow Wave,'' Phys. Fluids **11**, No. 11, pp. 3512–3523.
[14] Roth G., and Katz J., 1999, ''Parallel Truncated Multiplication and Other Methods for Improving the Speed and Accuracy of PIV Calculations,'' FEDSM-6998, Proc. ASME Fluids Eng. Conf., San Francisco.
[15] Roth, G. and Katz, J., 2000, ''Five Techniques for Increasing the Speed and Accuracy of PIV Interrogation,'' Meas. Sci. Technol. **12**, p. 238–245.
[16] Dong, R., Chu, S., and Katz, J., 1992, ''Quantitative Visualization of the Flow Structure within the Volute of a Centrifugal Pump, Part B: Results,'' ASME J. Fluids Eng. **114**, No. 3, pp 396–403.
[17] Roth G., Hart, D., and Katz J., 1995, ''Feasibility of Using the L64720 Video Motion Estimation Processor (MEP) to Increase Efficiency of Velocity Map Generation for Particle Image Velocimetry,'' ASME/EALA Sixth Int. Conf. on Laser Anemometry, Hilton Head, South Carolina.
[18] Sridhar, G., and Katz, J., 1995, ''Lift and Drag Forces on Microscopic Bubbles Entrained by a Vortex,'' Phys. Fluids **7**, No. 2, pp. 389–399.
[19] Adrian, R. J., 1991, ''Particle-imaging Techniques for Experimental Fluid Mechanics,'' Annu. Rev. Fluid Mech. **23**, 261–304.
[20] Japikse, D., 1998, ''Rotating Stall Investigations Expand,'' SPIN, **7**, pp. 4–5.
[21] Sinha, M., 1999, ''Rotor-Stator Interactions, Turbulence Modeling and Rotating Stall in a Centrifugal Pump with Diffuser Vanes,'' Ph.D. dissertation, The Johns Hopkins University, Baltimore, MD.
[22] Johnston, J. P., and Dean, R. C., 1966, ''Losses in Vaneless Diffusers of Centrifugal Compressors and Pumps,'' ASME J. Eng. Power **88**, pp. 49–62.
[23] Iversen, H. W., Rolling, R. E., and Carlson, J. J., 1960, ''Volute Pressure Distribution, Radial Forces on the Impeller, and Volute Mixing Losses of a Radial Flow Centrifugal Pump,'' ASME J. Eng. Power **82**, pp. 136–144.